

Czech Technical University in Prague
Faculty of Civil Engineering

České vysoké učení technické v Praze
Fakulta stavební

Ing. Jan Vorel, Ph.D.

**Calibration and Validation of Material Models
for Concrete**

Kalibrace a validace materiálových modelů pro beton

SUMMARY

Concrete is undoubtedly the most important and widely used construction material of the last centuries. Yet, mathematical models that can accurately capture the particular material behaviour under all loading conditions of significance are scarce at best. Although concepts and suitable models have existed for quite a while, their practical significance is low due to the limited attention to calibration and validation requirements and the scarcity of robust, transparent and comprehensive methods to perform such tasks. In addition, issues such as computational cost, difficulties associated with calculating the response of highly nonlinear systems, and, most importantly, lack of comprehensive experimental data sets have hampered progress in this area. This lecture attempts to promote the use of advanced concrete models by (a) providing a comprehensive set of concrete test data, cast from the same batch, available for model development, calibration, and validation, and (b) by presenting preliminary calibration and validation results for selected material models. Data included in the database comprise flexure tests of four sizes, direct tension tests, confined and unconfined compression tests, Brazilian splitting tests of five sizes, and loading and unloading data. For all specimen sets the nominal stress-strain curves and crack patterns are provided.

SOUHRN

Beton je nepochybně nejvíce rozšířený stavební materiál používaný během posledních století. Materiálové modely správně popisující chování betonu pro různé typy zatížení jsou vzácné. I když existují vhodné modely, jejich využití je často limitováno určením správných materiálových parametrů a jejich ověřením. Navíc, některé modely mají značnou výpočetní náročnost spojenou jak s matematickou formulací, tak s velikostí řešeného systému rovnic. Cílem přednášky je podpořit používání vhodných pokročilých modelů pomocí (a) poskytnutím velké sady experimentálních dat pro beton (všechny vzorky ze stejné dávky betonu), (b) předběžné výsledky kalibrací a validací vybraných materiálových modelů. Data obsažená v prezentované databázi se skládají ze tříbodového ohybu vzorků o různé velikosti, prostého tahu a tlaku, tlakové zkoušky za omezení příčné deformace, zkoušky v příčném tahu, atd. Pro všechny zkoušky jsou poskytnuty zatěžovací diagramy.

Keywords

concrete; fracture mechanics; failure; material models; experiments; calibration; validation

Klíčová slova

beton; lomová mechanika; porušení; materiálové modely; experimenty; kalibrace; validace

CONTENTS

Summary (english)	2
Souhrn (czech)	3
Keywords (english)	4
Klíčová slova (czech)	4
Chapter 1: Introduction	6
Chapter 2: Review of State of the Art models	6
2.1 Continuum based numerical models	7
2.2 Lattice Discrete Particle Model	10
Chapter 3: Experimental investigation	11
3.1 Mix properties and curing	13
3.2 Detailed description of tests	14
3.3 Overview of material properties	19
Chapter 4: Numerical simulations	19
4.1 Calibration	21
4.2 Validation	21
Chapter 5: Conclusions	24
Acknowledgements	25
References	25
Curriculum vitae	30

1 INTRODUCTION

As evident from the short review presented in the next chapter, many different concrete material models are available in the literature. However, the challenge that still remains is selecting the model that is most suitable for a given application, and obtaining the required input parameters. These can either have direct physical meaning or be solely model parameters that have to be inversely identified. However, in all cases sufficient experimental data are required to uniquely determine and finally validate the model parameters. This entails the availability of data of all required test types with sufficient number of samples to yield statistically meaningful results. Required tests include, but are not limited to, uniaxial compression, confined compression or triaxial tests, and direct or indirect tension tests. From these tests, strength and modulus information as well as hardening parameters can be derived. Due to the brittle nature of concrete indirect tension tests such as three-point-bending or splitting are generally preferred. In order to ensure unique softening parameters, softening post-peak data for at least two sizes [41] or alternatively two different types of tests should be obtained. Further tests are required if predictions under high loading rates or extreme environmental conditions have to be carried out. While for established models the predictive capabilities can be assumed to be satisfactory after calibration, new models also need to be validated. This step includes a subdivision of tests and specimens into sub-populations for calibration and prediction, where a random subset (typically $1/2$ to $2/3$) is allocated to calibration and the rest (ideally encompassing tests of all types) are used for prediction and validation.

Therefore, this lecture is focused on description of selected concrete material models (Chapter 2) and their calibration and validation (Chapter 4) against the experimental data obtain during the broad experimental campaign, see Chapter 3.

2 REVIEW OF STATE OF THE ART MODELS

Rapid progress in material science has led to the development of many new building materials with novel properties in recent years. However, concrete still remains the most favourable building material for its versatility and durability. Two of the main advantages of concrete are its high compressive strength and that it can be cast on the construction site into a variety of shapes and sizes. The most prominent disadvantages of concrete and other cementitious materials are their brittle failure behaviour in tension and low tensile strength.

The tensile behaviour of concrete and other quasi-brittle materials, often

also called strain softening materials, is characterised by crack propagation which causes a loss of carrying capacity with increasing deformation. This behaviour is typically described by non-linear fracture mechanics and suitable strain softening laws, characterised by the total fracture energy G_F or, equivalently, by Hillerborg's characteristic length [35, 34], $l_{ch} = EG_F/f_t'^2$ (E = Young's modulus; f_t' = tensile strength) which was derived based on Irwin's approximation for the size of the plastic zone in ductile materials [11, 38]. The strain softening is responsible for the dependence of structural strength on structural size [11] and thus must be properly captured by the numerical model.

Concrete behaviour in compression is even more complicated and depends on the level of confinement. Under low or no confinement, the compressive behaviour is characterised by a strain-softening. However, with increasing confinement, the behaviour varies from strain-softening to strain-hardening accompanied by a significant ductility [36, 5, 30, 8, 17].

Over the years many constitutive models have been developed to describe the behaviour of concrete based on the concepts of plasticity [40, 33], damage mechanics [6, 16] or fracture mechanics [11, 16]. They are typically formulated in tensorial (classical continuum based theory) or vectorial form (e.g., microplane theory, discrete particle models) [52, 42].

The present lecture deals with four continuum based numerical models (Concrete Damage Plasticity Model [32, 31], Fracture–Plastic Constitutive Model (CC3DNonLinCementitious2) implemented in **ATENA**¹ software [20], microplane M4 [12, 28] and microplane M7 [19]) and one lattice discrete particle model [26]. To provide a certain comparison between these numerical models, their calibration and validation with respect to experimental data [37, 53] are presented. Note that all models, except CC3DNonLinCementitious2, are implemented in the Multiscale-multiphysics Analysis of the Response of Structures (**MARS**²) computational environment [46] which is a powerful and robust object-oriented solver for simulating the mechanical response of structural systems subjected to short duration events. It employs an explicit time integration scheme for solving the equation of motion of large systems.

2.1 Continuum based numerical models

For continuum formulations, objectivity of the solution and independence of the numerical solution upon the finite element discretization have to be either inherent to the constitutive model, as for example in the case of high order [27] and nonlocal [39, 7] models, or must be imposed using regularisation

¹ <http://www.cervenka.cz/>

² <http://mars.es3inc.com/>

techniques such as the crack band approach [9, 11]. Methods that do not suffer from mesh sensitivity are also the ones accounting for strain softening through the insertion of cohesive discrete cracks [35, 45, 44].

2.1.1 Fracture–plastic constitutive model (CC3DNonLinCementitious2)

This constitutive material model is implemented in **ATENA** commercial software. The fracture-plastic model combines constitutive models for tensile fracturing and compressive plastic behaviour. The fracture behaviour is described by means of the classical orthotropic smeared crack formulation utilising fixed or rotated crack concepts, and crack band model employing Rankine failure criterion and exponential softening. The hardening/softening plasticity model is based on Menétrey-Willam failure surface. The return mapping algorithm for the integration of constitutive equations is implemented. The model can be employed to simulate concrete cracking, crushing under high confinement, and crack closure due to crushing in other material directions [20].

2.1.2 Concrete damage plasticity model

The concrete damage plasticity model (CDPM) based on the combination of damage and plasticity was developed to analyse the concrete failure [32, 31]. The plasticity part is based on the effective stress and the damage model is driven by the plastic and elastic strain. This constitutive model is capable of describing the important characteristics of the failure process of concrete subjected to multiaxial loading. The model describes well the increase in strength and displacement capacity for increasing confinement levels. To achieve the mesh-independent results the crack band approach is utilised. Note that the augmented version of the model (CDPM2), presented in [32], is employed in this study. The main differences, compare to the previous version (CDPM1), are (a) the introduction of two isotropic damage variables for tension and compression (single damage parameter for both tension and compression in CDPM1); (b) the hardening in the nominal post-peak regime.

2.1.3 Microplane Models

The microplane model, conceived in [13, 10], is a material constitutive model for progressive softening damage. Its advantage over the classical tensorial constitutive models is that it can capture the oriented nature of damage such as tensile cracking, slip, friction and compression splitting, as well as the orientation of fiber reinforcement. Another advantage is that the anisotropy of materials such as gas shale or fiber composites can be effectively represented.

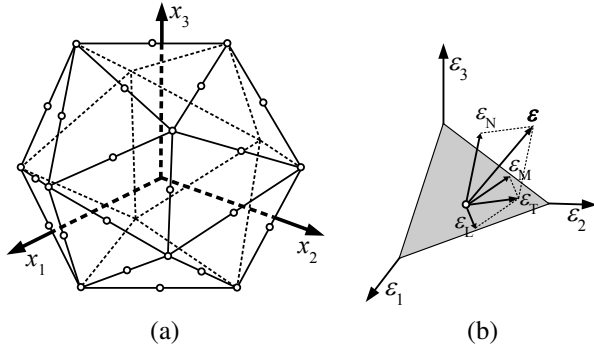


Figure 2.1: Microplane model: (a) distribution of integration points (microplane normals) - system of 21 microplanes per hemisphere; (b) microplane strain components

To prevent unstable strain localisation (and spurious mesh sensitivity in finite element computations), this model must be used in combination with some nonlocal continuum formulation (e.g., the crack band model). The basic idea of the microplane model is to express the constitutive law not in terms of tensors, but in terms of the vectors of stress and strain acting on planes of various orientations called the microplanes (Fig. 2.1). The use of vectors was inspired by G.I. Taylor's idea in 1938 [52] which led to Taylor models for plasticity of polycrystalline metals [4, 18, 47]. But the microplane models [13, 10, to cite a few] differ conceptually in two ways.

Firstly, to prevent model instability in post-peak softening damage, the kinematic constraint must be used instead of the static one. Thus, the strain (rather than stress) vector on each microplane is the projection of the macroscopic strain tensor. Secondly, a variational principle (or the principle of virtual work) relates the stress vector components on the microplanes to the macro-continuum stress tensor to ensure equilibrium.

Microplane M4 In the microplane model M4 [12], the constitutive relation in each microplane is defined by 1) incremental elastic relation and 2) stress-strain boundaries (softening yield limits) that cannot be exceeded. As pointed out in [28], the original formulation shows the erroneous behaviour in the uniaxial tension. Therefore, the original formulation of the microplane model M4 [12] was modified by introducing a no-split of the normal component for the dominant tensile failure (removing the tensile volumetric boundary) and by imposing the shear boundary on the shear stress resultant instead of on the single shear components individually [28]. Moreover, to improve the pre-

diction performance of the microplane model M4, two free parameters were added. One of these parameters can modify the slope of the softening branch of the uniaxial tensile or compression stress-strain curve and the other is able to set a different ratio between the tensile and the compression strength. This modified material model is utilised in the presented work.

Microplane M7 The microplane model M7 [19] is a follow-up of the previous versions from M0 to M6. The basic mathematical structure of M7 is logically correlated to thermodynamic potentials for the elastic regime, the tensile and compressive damage regimes, and the frictional slip regime. Based on the previous versions of the microplane model, it was realised that the volumetric-deviatoric split of strains is inevitable for distinguishing between compression failures at low and high confinement. In model M7, the key idea is to apply this split only to the microplane compressive stress-strain boundaries. The sum of these components is then compared with the total normal stress from the microplane constitutive relation. This avoids using the split of the elastic strains and of the tensile stress-strain boundary, which caused various troubles in M3–M6, e.g., excessive lateral strains and stress locking in far postpeak uniaxial extension, poor representation of unloading and loading cycles, and inability to represent high dilatancy under postpeak compression in lower-strength concretes. To accurately capture the differences between high hydrostatic compression and compressive uniaxial strain, the compressive volumetric boundary is dependent on the principal strain difference. [19]

2.2 Lattice Discrete Particle Model

Another class of models often used to simulate quasi-brittle materials is based on lattice or particle formulations in which materials are discretised “a priori” according to an idealisation of their internal structure (Fig. 2.2(a)). The unknown displacement field for discrete models is not continuous but only defined at a finite number of points which represent the centres of aggregate particles. Particle size and size of the contact area among particles, for particle models, as well as lattice spacing and cross sectional area, for lattice models, equip these types of formulations with inherent characteristic lengths and they have the intrinsic ability of simulating the geometrical features of material internal structure. This allows an accurate simulation of damage initiation and crack propagation at various length scales at the expense of increased computational cost.

Earlier attempts to formulate particle and lattice models for fracture are reported in [22, 23, 24, 21, 14] while the most recent developments were

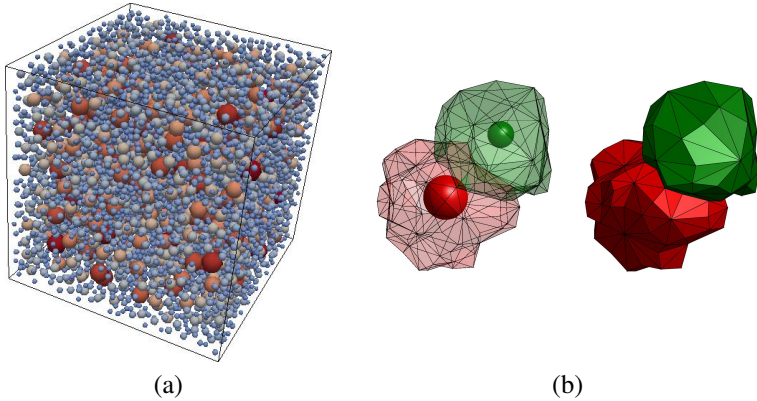


Figure 2.2: LDPM: (a) particle distribution; (b) cells for two adjacent aggregate particle

published in a Cement Concrete Composites special issue [21]. A comprehensive discrete formulation for concrete was recently proposed by Cusatis and coworkers [26, 25, 50, 51] who formulated the so-called Lattice Discrete Particle Model (LDPM) for which discrete compatibility and equilibrium equations are used to formulate the governing equations. A noticeable feature of LDPM is its ability to simulate a granular microstructure through a system of polyhedral particles connected through a three-dimensional lattice. Such particles can be placed randomly across the volume in accordance with a prescribed grain size distribution, thus enabling the direct representation of a heterogeneous system of grains surrounded by a bonding agent. Particle contact behaviour represents the mechanical interaction among adjacent aggregate particles through the embedding mortar (Fig. 2.2(b)). LDPM was calibrated, and validated against a large variety of loading conditions in both quasi-static and dynamic loading conditions and it was demonstrated to possess superior predictive capability.

3 EXPERIMENTAL INVESTIGATION

This lecture also focuses on the discussion of relevant tests for the calibration and validation of concrete models. This chapter summarises a comprehensive set of tests including uniaxial compression, confined compression and size-effect tests in three-point bending and splitting. All specimens were cast from the same batch and tested at an age of more than 400 days with the exception of standard 28-day compressive strength tests, thus significantly re-

ducing the influence of ageing. The raw data obtained in more than 257 tests have been pre-processed to provide statistical indicators for material properties and mean response curves for all types of tests, including post-peak softening.¹

Although the scientific literature contains an abundance of experimental data covering different phenomena and mechanisms, the number of publications reporting response curves for uniaxial compression, confined compression and indirect tension of the same concrete are limited, and virtually none simultaneously provide post-peak response for various sizes.

This investigation represents an extension of a size-effect investigation in three-point bending conducted by Hoover et al. [37] during which a total of 164 concrete specimens were cast in one batch (see section 3.1) in early 2011 and tested in 2012. A similar investigation dedicated to the fracture properties of self-consolidating concretes of various compositions is presented in Beygi et al. [15]. Following the work in [37], an additional 105 specimens were cut from the remaining shards in order to supplement, among other things, confined compression tests, Brazilian splitting tests, direct tension tests and hysteretic loading-unloading tests. The crack pattern was documented photographically and digitised by photogrammetric means for all fracture tests of the initial and extended investigation.

Response curves for the following tests are available:

- 128 three-point bending tests of 400 day old geometrically scaled unreinforced concrete beams of four sizes with a size range of 1:12.5 including un-notched specimens and beams with relative notch depths of $\alpha = a/D = 0.30, 0.15, 0.075, 0.025$, see Fig. 3.1(a);
- 12 centrally and eccentrically loaded 466 day old three-point bending specimens of size $D = 93$ mm according to Fig. 3.1(a), with and without unloading cycles in the softening regime;
- 40 Brazilian splitting tests, of roughly 475 day old prismatic specimens of 5 sizes with a size range of 1:16.7, see Fig. 3.1(b);
- 12 standard ASTM modulus of rupture tests [3] at 31 days and 400 days;
- 24 uniaxial compression tests of 3"x6" (75x150 mm) cylinders at 31 days and 400 days, see Fig. 3.1(c);
- 4 confined compression tests of 560 day old cored cylinders with $D = 50$ mm and $L = 40$ mm including 4 unconfined uniaxial compression tests of cored companion specimens;

¹ The complete collection of pre-processed response curves as well as the raw data are freely available at <http://www.baumat.boku.ac.at/comprtest.html>.

- 22 uniaxial compression tests of approximately 470 day old cubes with $D = 40$ mm and $D = 150$ mm, loaded partly monotonically and partly with several loading-unloading cycles in the softening regime, see Fig. 3.1(d);
- 6 uniaxial compression tests of approximately 950 day old cubes with $D = 40$ mm;
- 6 uniaxial tension tests of approximately 950 day old prisms;
- 11 torsion tests of prisms with $W = 40$ mm and $D = 40, 60, 80$ mm, see Fig. 3.1(e).

During these tests the stability problem has been considered in order to obtain the post-peak softening response. Choosing the right setup and the right control test mode is necessary to avoid the "snap-back" instability. Therefore, full or partial post-peak data are available for all tests except the ASTM modulus of rupture tests and the confined compression tests.

Due to the multitude of sizes and specimen geometries all plots are presented in the form of nominal stress σ_N versus nominal strain ε_N plots. Their definitions are for the:

- uniaxial tests: $\sigma_N = F/A$, $\varepsilon_N = \Delta L/L$;
- bending tests: $\sigma_N = M_F/S$, $\varepsilon_N = CMOD/D$;
- torsional tests: $\sigma_N = rM_T/J_T$, $\varepsilon_N = \theta' r$;

where F = force, A = cross section, M_F = bending moment, S = elastic section modulus, $CMOD$ = crack mouth opening displacement, r = eccentricity, M_T = torque, J_T = torsional moment of inertia, θ' = rate of the angle of twist as defined in [53], ΔL = variation of length and L = initial length.

3.1 Mix properties and curing

All 164 specimens of the initial investigation (128 beams, 12 ASTM beams, 24 cylinders) were cast in one batch of ready-mixed concrete with a specified compressive strength $f'_c = 31$ MPa. A more detailed description of mixing proportions and casting procedure is reported in [37, 53]. The concrete is characterised by pea gravel as coarse aggregate with a maximum diameter of 10 mm, a water-cement ratio $w/c = 0.41$, and a water-binder ratio $w/b = 0.35$. All the specimens used for the additional investigation were cut or cored out from the remaining shards of the original investigation [37].

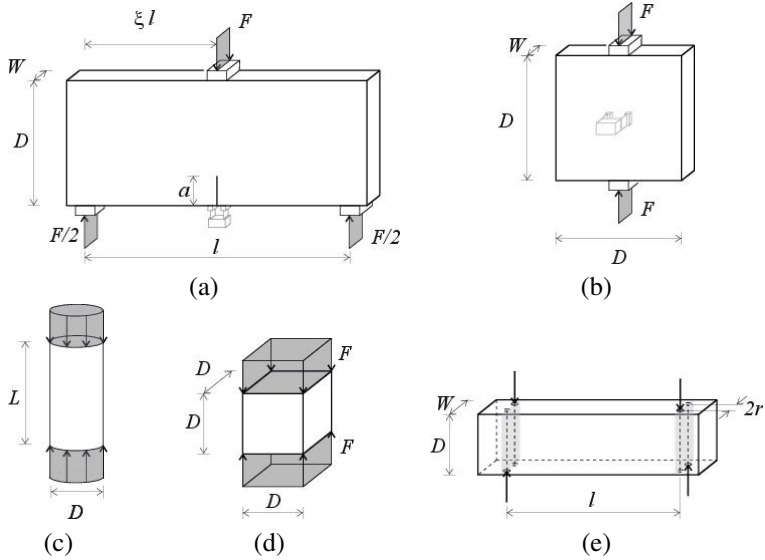


Figure 3.1: Specimen geometry: (a) three point bending tests; (b) Brazilian splitting tests; (c) unconfined compression tests of cylinders; (d) unconfined compression tests of cubes; (e) torsion tests

3.2 Detailed description of tests

The specific test setup and data analysis description can be found in [53]. In general, the tests were performed on servo-hydraulic closed-loop load frames with suitable load capacities. Moreover, during specimen preparation all relevant dimensions were rigorously recorded. To ensure unbiased and objective results, all presented data are processed automatically.

3.2.1 Flexural fracture by three-point bending

Characterisation of flexural fracture is topic that covers the major part of the presented investigation. In particular, the size dependency of flexural strength and toughness are of interest. The studied parameters were: the relative notch depth, relative load eccentricity (the parameter ξ in Fig. 3.1(a)) and the modulus reduction in the softening regime. In total, 128 geometrically scaled beams of four sizes with a size range of 1:12.5 were tested. In addition to the specimens with different notch depths [37], un-notched specimens were also investigated. At least six specimens were tested for each size and notch depth combination (more for the smallest two sizes due the larger inherent

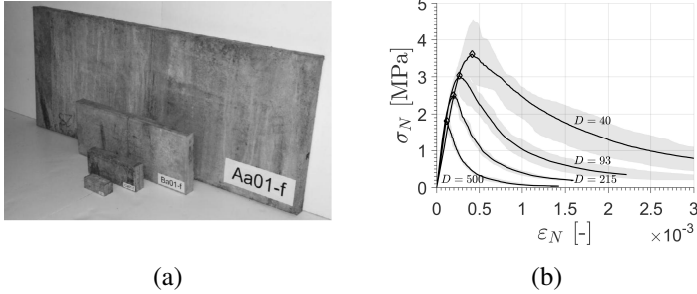


Figure 3.2: Notched three-point bending test ($\alpha = 0.3$): (a) view of different sizes of beams; (b) mean responses of the notched specimens

scatter). A visual overview of the set of beams can be seen in Fig. 3.2(a). The specimen geometry is shown in Fig. 3.1(a).

All dimensions were geometrically scaled except the notch width and the specimen thickness W . At an age of 96 days the notches were cut with a diamond coated band saw. Approximately 400 days after casting, all 128 beams of the bending size effect investigation were tested within a span of 11 days. The chosen stable mode of control was Crack Mouth Opening Displacement (CMOD) for notched specimens and average tensile strain for un-notched beams. For the purpose of this investigation, nominal stress σ_N for bending specimens is defined according to the beam theory. For the notched specimens the nominal strain ε_N is based on the measured opening of the extensometer while for un-notched specimens an engineering strain definition is chosen. The corresponding plots for notched specimens with relative notch length of $\alpha = 0.3$ are shown in Fig. 3.2(b).

The macroscopic strength of specimens without an initial notch is influenced mostly by the material heterogeneity which manifests itself in widespread crack localization on the tension side, see the photogrammetrically obtained crack path distribution of all un-notched specimens in Fig. 3.3(a). Fig. 3.3(b) shows the crack distributions of notched beams with all cracks emanating from the notch tip.

Data concerning the bending shear interaction are available in the form of eccentrically loaded un-notched beams of the second smallest size with $D = 93$ mm.

3.2.2 Unconfined compression

Compression tests are the most traditional tests used to characterise concrete and they are typically performed on cylinders or cubes. In the case of Euro-

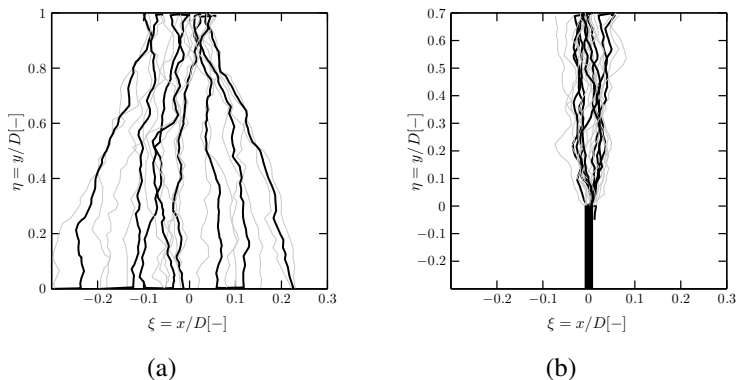


Figure 3.3: Example of crack pattern in three-point bending ($D = 93$ mm) for: (a) un-notched specimens; (b) notched specimens ($\alpha = 0.3$)

code [1, 2] both cubes of 150 mm side length and cylinders with 150 mm diameter and 300 mm height are tested using 4 LVDT to measure the variation of the length ΔL . The derived cylinder strength f_{cyl} and cube strength f_{cu} are used to specify concrete with the typical label “ Cf_{cyl}/f_{cu} ”. Unconfined compression tests, in addition to the material’s uniaxial compressive strength, also provide an insight into the softening behaviour already starting before the peak-load is reached.

During the investigation twelve 75x150 mm cylinders were tested, each after 31 days and after 400 days. Additionally, eight 150 mm cubes were cut out of the undamaged parts of the ASTM modulus of rupture specimens and fourteen 40 mm cubes were cut from the remainders of the three-point bending size effect investigation. The tests were performed at an age of approximately 470 days.

3.2.3 Confined compression

In order to perform confined tests, high passive confinement was achieved using thick-walled steel jackets which dimensions were: 88.6 mm high, 47.3 mm of inner diameter and 14.15 mm of thickness, (Fig. 3.4(a)). Four confined and four unconfined but otherwise identical specimens were tested. The force, the piston stroke and the circumferential expansion of the steel jacket as indicator for the confinement, are available from these tests. The unconfined companion specimens (without steel jacket) with an otherwise identical setup to maintain the compliance contribution of the setup were carried out as well. Unfortunately, the response under strong confinement is strongly

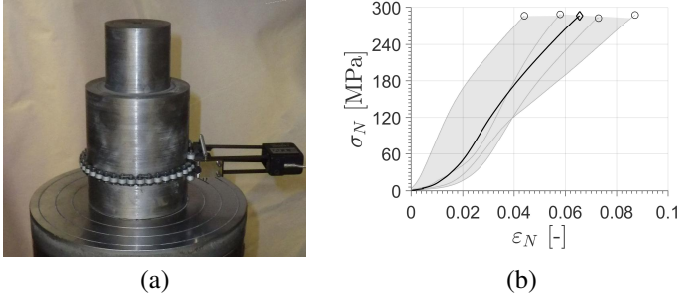


Figure 3.4: Confined compression test: (a) setup ; (b) mean response

biased by the grouting material and friction, thus reducing the value of this data, see Fig. 3.4(b).

3.2.4 Brazilian splitting test

Another commonly used test is the so-called Brazilian splitting test where the specimen is loaded in compression, leading to lateral expansion and ultimately to tensile failure perpendicular to the maximum principle stress direction. The specimens are supported and loaded by wooden or steel bearing strips with pre-determined dimensions. Within this investigation prismatic specimens according to Fig. 3.1(b) of five sizes with constant thickness were tested.

The specimen response is plotted in terms of nominal stress σ_N and nominal strain ϵ_N for all five sizes and wooden bearing strips in Fig. 3.5(a). For the purpose of this investigation nominal stress σ_N is defined as the maximum tensile stress $\sigma_{max}(\beta = w/D)$ according to Rocco et al. [49, 48]. Nominal strain is defined as the engineering strain utilising the extensometer opening u and the gauge length. The normalised crack patterns for the specimens with size $D = 93$ mm and supported by wooden bearing strips can be observed in Fig. 3.5(b).

3.2.5 Tension

Single notch tension specimens were cut from undamaged pieces of the original size effect investigation on approximately 950 day old concrete prisms. A notch with a relative depth $\alpha = a/D = 0.25$ (see Fig. 3.6(a)) was made in order to ensure localisation of the crack in the center cross-section of the beam and also to control the test by crack mouth opening. The boundary conditions are characterised by fully clamped support on one side and pin

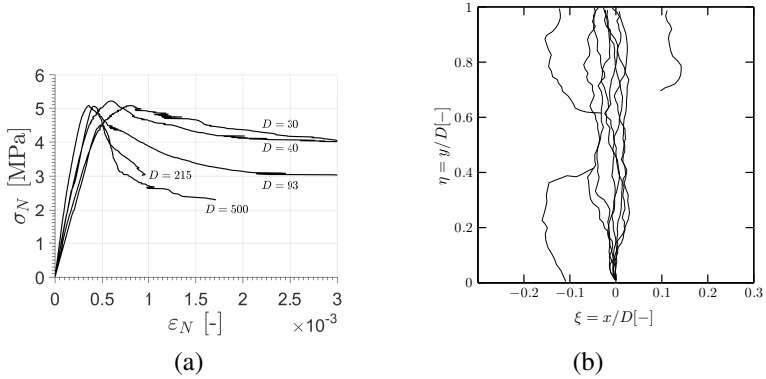


Figure 3.5: Brazilian splitting tests: (a) mean responses of specimens with different sizes [mm]; (b) crack pattern for $D = 93$ mm

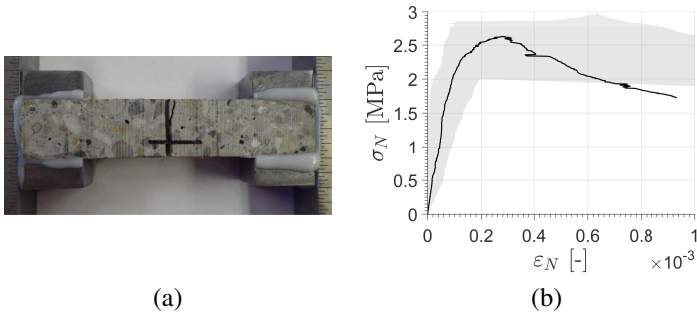


Figure 3.6: Single notch tension test; (a) setup; (b) mean response

support on the other end. Nominal stress is defined according to the elastic solution of un-notched specimens while nominal strain is defined as the engineering strain utilising the extensometer opening u and the gauge length. The resulting nominal stress-strain diagram is given in Fig. 3.6(b).

3.2.6 Torsion

Pure torsion test data are available for three cross-sections of width $W = 40$ mm and height $D = 40, 60, 80$ mm. The specimens were loaded by two opposing moment couples with an eccentricity of 20 mm (Fig. 3.1(e)). Free rotation of all four loading and support points was guaranteed by ball bear-

Table 3.1: Material properties extracted from cylinder, ASTM modulus of rupture, and three-point bending tests (age of around 400 days)

material property		unit	mean	CoV [%]
compr. cyl. strength	$f_{cyl,75}$ (31 days)	MPa	46.5	3.2
compr. cyl. strength	$f_{cyl,75}$	MPa	55.6	3.7
compr. cube strength	$f_{cu,150}$ (470 days)	MPa	57.1	5.5
ASTM m. of rupture	f_r	MPa	8.3	3.6
m. of elast., 75 mm cyl	$E_{cyl,75}$	GPa	34.38	3.9
Poisson's ratio	ν	-	0.172	10.0
initial fracture energy	G_f	N/m	51.87	-
characteristic length	c_f	m	23.88	-
total fracture energy	G_F	N/m	96.94	16.9

ings. The span length l was chosen to be 160 mm for the square cross-section and 240 mm otherwise.

3.3 Overview of material properties

The basic concrete properties have been extracted from various tests performed at different ages. For convenience a summary is provided in Table 3.1, see also [37, 53]. Compressive strength was determined based on 75x150 mm cylinders and 150 mm cubes. The reported Poisson ratio was determined based on the circumferential expansion of standard cylinders in compression [37] and the fracture properties were obtained by fitting of Type 2 size effect law [37].

4 NUMERICAL SIMULATIONS

The preliminary results of calibration and validation of different numerical models, introduced in Chapter 2, are presented hereafter. As already mentioned, all utilised models, except CC3DNonLinCementitious2 (**ATENA**), are implemented in the **MARS** computational environment to control and limit differences in implementations and solvers. The experimentally obtained set of data (see Chapter 3) is divided into two subsets: (a) data for calibration - three-point bending tests for $\alpha = 0.3$ and $D = 93$ mm; unconfined compression cube test $D = 40$ mm; confined cylinder compression test; (b) data for validation - remaining experimental data in Chapter 3. In general, the approach used to study the material models can be characterised by two steps:

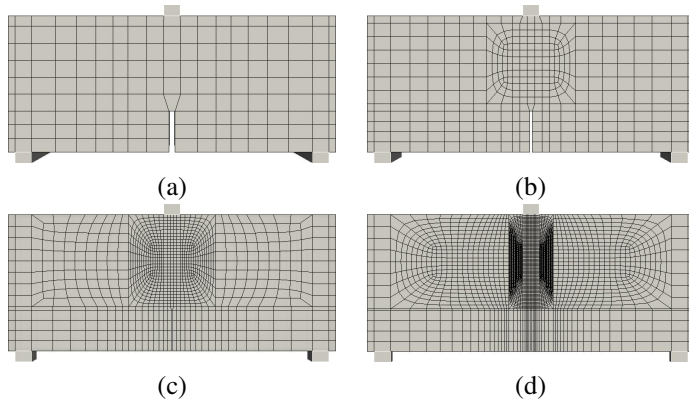


Figure 4.1: Meshes for three-point bending tests ($\alpha = 0.3$): (a) $D = 40$ mm; (b) $D = 93$ mm; (c) $D = 215$ mm; (d) $D = 500$ mm

1. calibration of each model based on the limited set of data which are usually available, i.e., determination of material parameters of each model;
2. verification of the model behaviour by comparing the results of numerical simulations with remaining experimental data not used for calibration, parameter adjustments are not permitted.

The consistent mesh is used for continuum based numerical simulations to minimise the mesh size and type influence. Linear 3D eight-node hexahedral solid finite elements with 8 integration points and size equal to 5 mm are utilised (Fig. 4.1), in the regions where the propagation of damage is expected, to avoid the discrepancies caused by the utilised regularisation approaches even though the regularisation based on the crack band approach is available for CDPM2, M4 and CC3DNonLinCementitious2 models.

The LDPM material model response is dependent on particle distribution. Therefore, each numerical curve is calculated as the average of three to five numerical simulations obtained on specimens with different meso-structure (e.g., different random particle configuration). The particle gradation follows the classical Fuller-Thompson distribution function [29] with the aggregate size limited to 4-10 mm, see [46].

Note that the results for microplane M4 are not available yet and are not presented in this lecture.

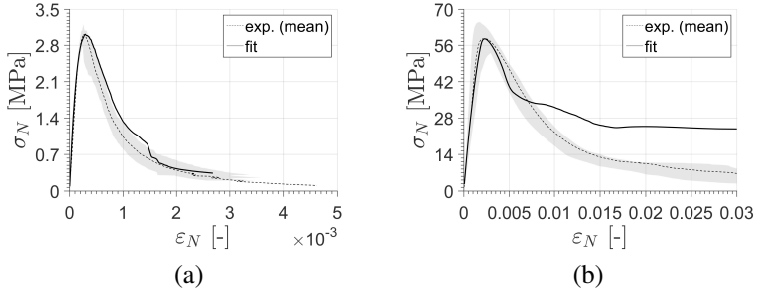


Figure 4.2: CC3DNonLinCementitious2 model (ATENA) calibration: (a) three-point bending test ($D = 93$ mm, $\alpha = 0.3$); (b) unconfined compression cube test ($D = 40$ mm)

4.1 Calibration

Calibration of model parameters is obtained through the best fitting of the complete load–displacement (opening) curves relevant to chosen experimental tests. These tests were chosen to mimic the commonly available test data. The best fitting was performed through a “trial and error” procedure based on a visual assessment of the agreement between the numerical result and the experimental data, see Figs. 4.2-4.5. It must be noted that not all experimental data to calibrate all material parameters are available (e.g., triaxial compression tests, etc.). Therefore, the relevant material parameters are either based on an “educated guess” or default values recommended by the corresponding authors. For the unconfined compression the load was applied through steel platens that are directly in contact with the specimens ends (high friction condition). This condition is simulated by the sliding with friction constraint, see [46]. In ATENA computational framework the CC3DInterface 3D interface was utilised. The calibrated material parameters can be found in [43].

4.2 Validation

In the present lecture, the preliminary results of validation are shown by comparing the numerical simulations with the experimental data that were not used in the calibration phase, i.e., three-point bending tests data ($D = 40, 93, 215$ mm, $\alpha = 0.3, 0.0$) and where possible the compression cube test for $D = 150$ mm, see Figs. 4.6-4.10.

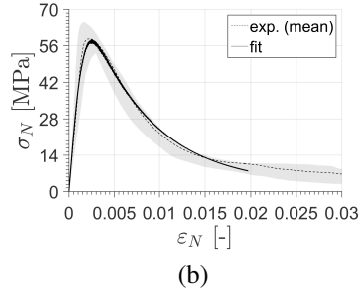
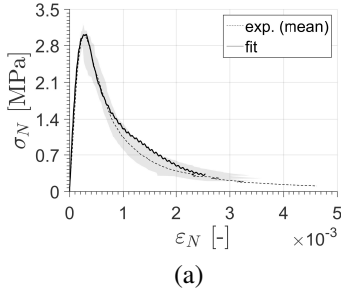


Figure 4.3: CDPM2 calibration: (a) three-point bending test ($D = 93$ mm, $\alpha = 0.3$); (b) unconfined compression cube test ($D = 40$ mm)

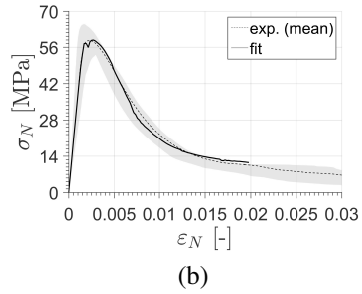
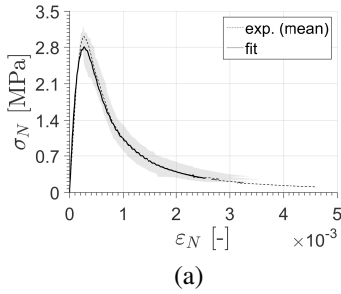


Figure 4.4: Microplane M7 calibration: (a) three-point bending test ($D = 93$ mm, $\alpha = 0.3$); (b) unconfined compression cube test ($D = 40$ mm)

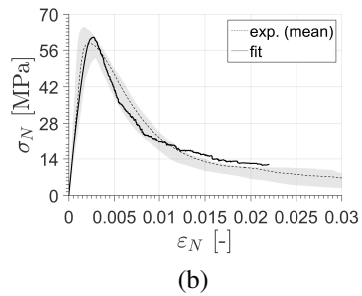
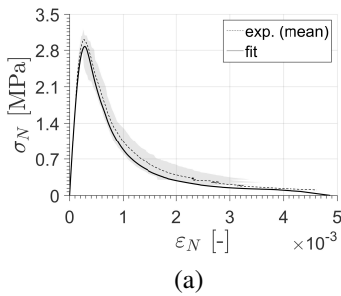


Figure 4.5: LDPM calibration: (a) three-point bending test ($D = 93$ mm, $\alpha = 0.3$); (b) unconfined compression cube test ($D = 40$ mm)

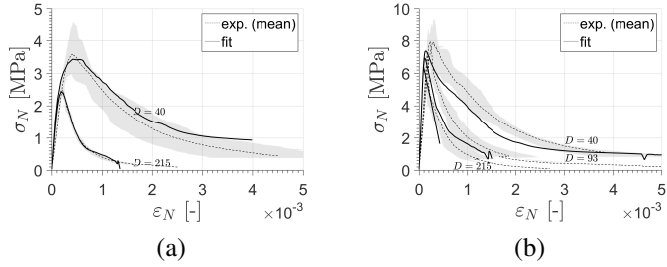


Figure 4.6: CC3DNonLinCementitious2 model (ATENA) validation: (a) three-point bending test ($\alpha = 0.3$); (b) three-point bending test ($\alpha = 0.0$, unnotched)

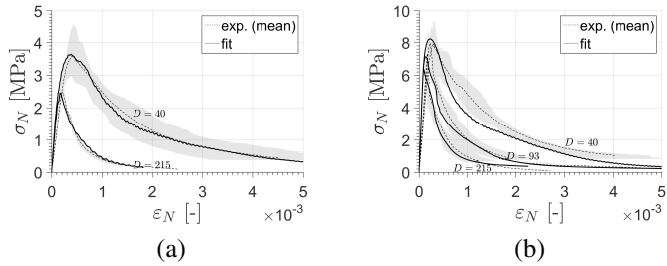


Figure 4.7: CDPM2 validation: (a) three-point bending test ($\alpha = 0.3$); (b) three-point bending test ($\alpha = 0.0$, unnotched)

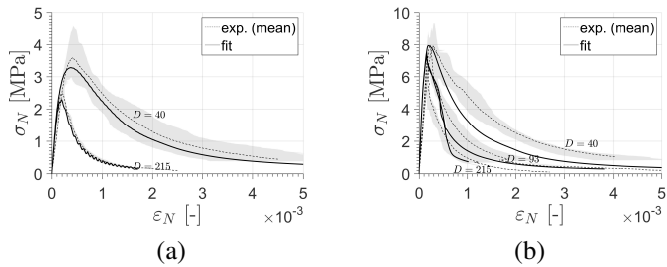


Figure 4.8: Microplane M7 validation: (a) three-point bending test ($\alpha = 0.3$); (b) three-point bending test ($\alpha = 0.0$, unnotched)

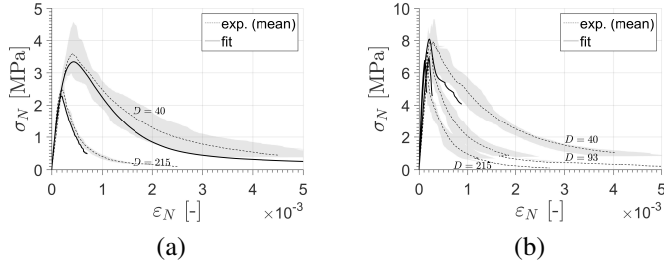


Figure 4.9: LDPM validation: (a) three-point bending test ($\alpha = 0.3$); (b) three-point bending test ($\alpha = 0.0$, un-notched)

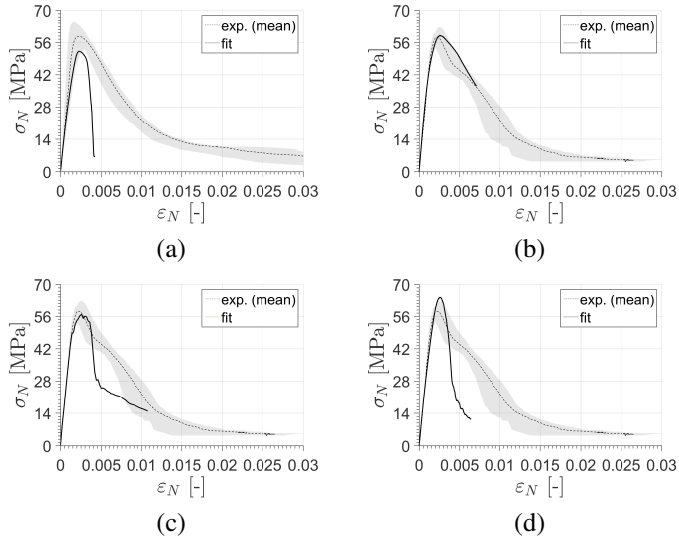


Figure 4.10: Unconfined compression cube test ($D = 150$ mm): (a) CC3DNonLinCementitious2 model; (b) CDPM2; (c) microplane M7; (d) LDPM

5 CONCLUSIONS

In order to realistically model the concrete behaviour, selected advanced material models are calibrated and validated against large set of experimental data. As can be seen from the preliminary results in the previous chapter, good agreement exists between the predicted responses and experimental

data. The major difference appears for the unconfined compression ($D = 150$ mm) which is probably caused by defined interface between the concrete and steel platens or inadequate model calibration in compression. The response of CDPM2 sufficiently fits the experimental data. All tested material models have the capability of capturing the size effect pronounced for the notched and un-notched three-point bending tests. However, still more numerical simulations have to be performed to assess different loading scenarios, e.g., torsion, eccentric three-point bending. Note that only limited set of data was used to calibrate the material models to mimic the commonly used practise. The calibration demands of each model are also different and often increase with number of fitted material parameters. The experimental data presented in Chapter 3 represents an ideal data source for model development, calibration and validation of concrete material models.

Only visual assessment of the agreement between the numerical result and the experimental data is employed in this lecture. The more objective indicators have to be defined to undoubtedly compare predictions of different numerical models. Such indicators should be objective, uncorrelated and independent of absolute value.

ACKNOWLEDGEMENTS

The financial support provided by the GAČR grant No. 15-10354S is gratefully acknowledged.

REFERENCES

- [1] Concrete - part 1: Specification, performance, production and conformity, 2000.
- [2] Eurocode 2: Design of concrete structures, part 1-1: General rules and rules for buildings, 2004.
- [3] ASTM. C293: standard test method for flexural strength of concrete (using simple beam with center-point loading), 2010.
- [4] S.B. Batdorf and B. Budiansky. A mathematical theory of plasticity based on the concept of slip. *NACA Technical Note*, 1949.
- [5] Z.P. Bažant, F.C. Bishop, and T.P. Chang. Confined compression tests

of cement paste and concrete up to 300 ksi. In *ACI Journal Proceedings*, volume 83. ACI, 1986.

- [6] Z.P. Bažant and L. Cedolin. *Stability of Structures: Elastic, Inelastic, Fracture and Damage Theories*. Oxford University Press, New York, 2nd edition, 1991.
- [7] Z.P. Bažant and M. Jirásek. Nonlocal integral formulations of plasticity and damage: survey of progress. *Journal of Engineering Mechanics*, 128(11):1119–1149, 2002.
- [8] Z.P. Bažant, J.J.H. Kim, and M. Brocca. Finite strain tube-squash test of concrete at high pressures and shear angles up to 70 degrees. *ACI Materials Journal*, 96(5):580–592, 1999.
- [9] Z.P. Bažant and B.H. Oh. Crack band theory for fracture of concrete. *Materials and Structures*, 16:155–177, 1983.
- [10] Z.P. Bažant and B.H. Oh. Microplane model for progressive fracture of concrete and rock. *Journal of Engineering Mechanics*, 111(4):559–582, 1985.
- [11] Z.P. Bažant and J. Planas. *Fracture and Size Effect in Concrete and other Quasibrittle Materials*. CRC Press, Boca Raton, Florida, 1998.
- [12] Zdenek P Bazant, Ferhun C Caner, Ignacio Carol, Mark D Adley, and Stephen A Akers. Microplane model m4 for concrete. i: Formulation with work-conjugate deviatoric stress. *Journal of Engineering Mechanics*, 126(9):944–953, 2000.
- [13] Z.P. Bažant. Microplane model for strain-controlled inelastic behaviour, chapter 3. *Mechanics of engineering materials, chapter 3*, 1984.
- [14] Z.P. Bažant, M.R. Tabbara, M.T. Kazemi, and G. Pijaudier-Cabot. Random particle model for fracture of aggregate or fiber composites. *Journal of Engineering Mechanics*, 116(8):1686–1705, 1990.
- [15] M.H.A. Beygi, M.T. Kazemi, I.M. Nikbin, and J.V. Amiri. The effect of water to cement ratio on fracture parameters and brittleness of self-compacting concrete. *Materials & Design*, 50:267–276, 2013.
- [16] Z. Bittnar and J. Šejnoha. *Numerical methods in structural mechanics*. ASCE Publications, 1996.

- [17] M. Brocca and Z.P. Bažant. Microplane finite element analysis of tube-squash test of concrete with shear angles up to 70. *International Journal for Numerical Methods in Engineering*, 52(10):1165–1188, 2001.
- [18] B. Budiansky and T.T. WU. Theoretical prediction of plastic strains of polycrystals. Technical report, DTIC Document, 1961.
- [19] F.C. Caner and Z.P. Bažant. Microplane model M7 for plain concrete: I. Formulation. *Journal of Engineering Mechanics*, 2012.
- [20] V. Červenka, L. Jendele, and J. Červenka. Atena program documentation. *Theory and User manual, Cervenka Consulting, Prague*, 2016.
- [21] G. Cusatis. Strain-rate effects on concrete behavior. *International Journal of Impact Engineering*, 38(4):162–170, 2011.
- [22] G. Cusatis, Z.P. Bažant, and L. Cedolin. Confinement-shear lattice model for concrete damage in tension and compression: I. Theory. *Journal of Engineering Mechanics*, 129:1439, 2003.
- [23] G. Cusatis, Z.P. Bažant, and L. Cedolin. Confinement-shear lattice model for concrete damage in tension and compression: II. Computation and validation. *Journal of Engineering Mechanics*, 129:1449, 2003.
- [24] G. Cusatis, Z.P. Bažant, and L. Cedolin. Confinement-shear lattice CSL model for fracture propagation in concrete. *Computer Methods in Applied Mechanics and Engineering*, 195(52):7154–7171, 2006.
- [25] G. Cusatis, A. Mencarelli, D. Pelessone, and J. Baylot. Lattice discrete particle model (LDPM) for failure behavior of concrete. II: Calibration and validation. *Cement and Concrete Composites*, 33(9):891–905, 2011.
- [26] G. Cusatis, D. Pelessone, and A. Mencarelli. Lattice discrete particle model (LDPM) for failure behavior of concrete. I: Theory. *Cement and Concrete Composites*, 33(9):881–890, 2011.
- [27] R. de Borst, M.A. Gutiérrez, G.N. Wells, J.J.C. Remmers, and H. Askes. Cohesive-zone models, higher-order continuum theories and reliability methods for computational failure analysis. *Int. J. Numer. Meth. Engng*, 60(1):289–315, 2004.
- [28] G. Di Luzio. A symmetric over-nonlocal microplane model m4 for fracture in concrete. *International journal of solids and structures*, 44(13):4418–4441, 2007.

- [29] W.B. Fuller and S.E. Thompson. The laws of proportioning concrete. *Transactions of the American Society of Civil Engineers*, 59:67–143, 1907.
- [30] T. Gabet, Y. Malécot, and L. Daudeville. Triaxial behaviour of concrete under high stresses: Influence of the loading path on compaction and limit states. *Cement and Concrete Research*, 38(3):403–412, 2008.
- [31] P. Grassl and M. Jirásek. Damage-plastic model for concrete failure. *International journal of solids and structures*, 43(22):7166–7196, 2006.
- [32] P. Grassl, D. Xenos, U. Nyström, R. Rempling, and K. Gylltoft. Cdpm2: A damage-plasticity approach to modelling the failure of concrete. *International Journal of Solids and Structures*, 50(24):3805–3816, 2013.
- [33] D.-J. Han. *Plasticity for structural engineers*. J. Ross Publishing, 2007.
- [34] A. Hillerborg. The theoretical basis of a method to determine the fracture energy G_f of concrete. *Materials and Structures*, 18(4):291–296, 1985.
- [35] A. Hillerborg, M. Modéer, and P.E. Petersson. Analysis of crack formation and crack growth in concrete by means of fracture mechanics and finite elements. *Cement and concrete research*, 6:773–782, 1976.
- [36] H.K. Hilsdorf, W.R. Lorman, and G.E. Monfore. Triaxial testing of nonreinforced concrete specimens. *Journal Testing & Evaluation*, 1(4), 1973.
- [37] C.G. Hoover, Z.P. Bažant, J. Vorel, R. Wendner, and M.H. Hubler. Comprehensive concrete fracture tests: Description and results. *Engineering Fracture Mechanics*, 114:92–103, 2013.
- [38] G.R. Irwin. *Fracture*, volume VI of *Encyclopaedia of physics*. Springer, Berlin , Germany, 1958.
- [39] M. Jirásek. Nonlocal models for damage and fracture: Comparison of approaches. *International Journal of Solids and Structures*, 35(31-32):4133–4145, 1998.
- [40] M. Jirásek and Z.P. Bažant. *Inelastic analysis of structures*. Wiley. com, 2002.
- [41] K.T. Kim, Z.P. Bažant, and Q. Yu. Non-uniqueness of cohesive-crack stress-separation law of human and bovine bones and remedy by size effect tests. *International Journal of Fracture*, 181(1):67–81, 2013.

- [42] T.H. Lin. *Theory of Inelastic Structures*. John Wiley & Sons, Inc., 1968.
- [43] M. Marcon, J. Vorel, G. Di Luzio, G. Cusatis, F. Caner, Z.P. Bažant, and R. Wendner. Constitutive modeling of concrete - comparison of the state of the art models. Paper before submission.
- [44] N. Moës, J. Dolbow, and T. Belytschko. A finite element method for crack growth without remeshing. *International Journal for Numerical Methods in Engineering*, 46(1):131–150, 1999.
- [45] A. Needleman and V. Tvergaard. An analysis of ductile rupture modes at a crack tip. *Journal of the Mechanics and Physics of Solids*, 35(2):151–183, 1987.
- [46] D. Pelessone. *MARS Manual*. ES3 Inc., 2016. <http://mars.es3inc.com/>.
- [47] J.R. Rice. Inelastic constitutive relations for solids: an internal-variable theory and its application to metal plasticity. *Journal of the Mechanics and Physics of Solids*, 19(6):433–455, 1971.
- [48] C. Rocco, G.V. Guinea, J. Planas, and M. Elices. Size effect and boundary conditions in the brazilian test: Experimental verification. *Materials and Structures*, 32(3):210–217, 1999.
- [49] C. Rocco, G.V. Guinea, J. Planas, and M. Elices. Size effect and boundary conditions in the brazilian test: theoretical analysis. *Materials and Structures*, 32(6):437–444, 1999.
- [50] E.A. Schaufert and G. Cusatis. Lattice discrete particle model for fiber-reinforced concrete. I: Theory. *Journal of Engineering Mechanics*, 138(7):826–833, 2011.
- [51] E.A. Schaufert, G. Cusatis, D. Pelessone, J. O’Daniel, and J. Baylot. Lattice discrete particle model for fiber-reinforced concrete. II: Tensile fracture and multiaxial loading behavior. *Journal of Engineering Mechanics*, 138(7):834–841, 2012.
- [52] G.I. Taylor. Plastic strain in metals. *J. Inst. Metals*, 63:307–324, 1938.
- [53] R. Wendner, J. Vorel, J. Smith, C.G. Hoover, Z.P. Bažant, and G. Cusatis. Characterization of concrete failure behavior: a comprehensive experimental database for the calibration and validation of concrete models. *Materials and Structures*, pages 1–24, 2014.

Ing. JAN VOREL, Ph.D.

Personal details

Name: **JAN VOREL**
Born: June 26, 1981, Czech Republic
Email: jan.vorel@fsv.cvut.cz

Activities

Research activities involve the field of computational mechanics. Special interest is focused on multi-scale analysis of heterogeneous materials and composites.

Experience

2014- CZECH TECHNICAL UNIVERSITY IN PRAGUE, Faculty of Civil Engineering, Czech Republic. Position: *Assistant professor*

2011-2012 NORTHWESTERN UNIVERSITY, USA. Position: *postdoc fellowship*. Supervisor: *Zdeněk P. Bažant*.

2009 STELLENBOSCH UNIVERSITY, Department of Civil Engineering, South Africa. Position: *research fellowship*. Supervisor: *William P. Boshoff*.

2006-2013 CZECH TECHNICAL UNIVERSITY IN PRAGUE, Faculty of Civil Engineering, Czech Republic. Position: *lecturer and research assistant*

Education

2009 DOCTOR OF PHILOSOPHY, Czech Technical University in Prague, Faculty of Civil Engineering, Czech Republic. Branch of study: *Physical and Material Engineering*

2006 MASTER OF SCIENCE (graduated with honors), Czech Technical University in Prague, Faculty of Civil Engineering, Czech Republic. Branch of study: *Building Structures*

Projects

Principal investigator or collaborator in 8 national and 2 international research projects.

2015- CTU in Prague. Project topic: *Advanced tools for the analysis of timber structures considering variability of model parameters*, GAČR 15-10354S

2014- BOKU Vienna. Project topic: *CDL for Life Cycle Robustness in Fastening Technology*, GAČR 15-10354S

Publications

Author and co-author of two book chapters, nineteen journal papers, four authorized softwares and more than fifty conference contributions.

Book chapters

- [1] M. Šejnoha, J. Vorel, M. Maršálková, and E. Grippon. *Civil and Structural Engineering Computational Technology*, volume 3 of *Selected Chapters of Mechanics of Composites Materials*, chapter Multi-scale modeling of textile reinforced ceramic composites, pages 145–187. Derc Publishing House, 2013.
- [2] M. Šejnoha, J. Vorel, R. Valenta, and J. Zeman. *Civil and Structural Engineering Computational Technology*, volume 28 of *Computational Science, Engineering and Technology Series*, chapter Virtual Experiments and a Statistically Equivalent Representative Volume Element for Macroscopic Constitutive Laws, pages 131–155. Saxe-Coburg Publications, 2011.

Journal papers (2016-2015)

- [1] L. Svoboda, S. Šulc, T. Janda, J. Vorel, and J. Novák. μ Mech micromechanics library. *Advances in Engineering Software*, 100:148–160, 2016.
- [2] J. Vorel and W.P. Boshoff. Computational modelling of real structures made of strain-hardening cement-based composites. *Applied Mathematics and Computation*, 267:562–570, 2015.
- [3] J. Vorel, E. Grippon, and M. Šejnoha. Effective thermoelastic properties of polysiloxane matrix based plain weave textile composites. *International Journal for Multiscale Computational Engineering*, 13(3):181–200, 2015.
- [4] R. Wendner, J. Vorel, J. Smith, C.G. Hoover, Z.P. Bažant, and G. Cusatis. Characterization of concrete failure behavior: a comprehensive experimental database for the calibration and validation of concrete models. *Materials and Structures*, 48(11):3603–3626, 2015.